

Deeper penetration of surface effects on particle mobility than on hopping rate in glassy polymer films

Chi-Hang Lam*

Department of Applied Physics, Hong Kong Polytechnic University, Hong Kong, China

(Dated: October 2, 2018)

Free surfaces in glassy polymer films are known to induce surface mobile layers with enhanced dynamics. Using molecular dynamics simulations of a bead-spring model, we study a wide variety of layer-resolved structural and dynamical properties of polymer films equilibrated at a low temperature. Surface enhancement on thermally induced particle hopping rate is found to terminate abruptly only about 5 particle diameters from the free surface. In contrast, enhancement on the net motions of particles measured at longer time scales penetrates at least 2 particle diameters deeper. The diverse penetration depths show the existence of a peculiar sublayer, referred to as the inner-surface layer, in which surface enhanced mobility is not caused by more frequent particle hops but instead by a reduced dynamic heterogeneity associated with diminished hopping anti-correlations. Confinement effects of the free surface thus provide a unique mechanism for varying the dynamic heterogeneity and hopping correlations while keeping the hopping rate constant. Our results highlight the importance of correlations among elementary motions to glassy slowdown and suggest that dynamic facilitation is mediated via perturbations to the correlations rather than the rate of elementary motions.

I. INTRODUCTION

The nature of glassy dynamics is a long-standing problem attracting intensive investigations [1–5]. Confinement effects on glassy thin films are widely studied in attempt to provide additional insights [5–8]. It has already been suggested early on, based on polymer thin film experiments, that surface layers with enhanced dynamics dominate thin film confinement effects [9, 10]. This is supported by molecular dynamics (MD) simulations [11, 12] and has been further established by more recent film flow experiments [13–15]. In particular, our experiments on short-chain polymer thin films in Ref. [13] have shown that a thin surface mobile layer exists on top of a glassy bulk layer. The dynamics of the surface layer follow an Arrhenius temperature dependence. This non-glassy nature of the surface layer is consistent with indications from earlier experiments [16, 17].

A main motivation of the study by Keddie et al. on polymer films was to cast light onto the fundamental origins of glass [9]. This has proved challenging due to complications including substrate influences and possible long-range elastic couplings by long polymer chains. Short-chain polymer films on supposedly non-slipping and non-permanently pinning substrates such as those used in Ref. [13] may thus provide the simplest scenario. Nevertheless, the origin and the detailed properties of the surface mobile layer are still controversial [18–22]. For simplicity, one often assume simple layer models in which both the surface mobile layer and the inner glassy layer have uniform properties separated by an abrupt boundary [9, 10, 13, 23, 24]. However, films are expected to have graded depth-dependent properties [25–27] as found in MD simulations [11, 12, 28–30].

It is long known from MD simulations that perturbations due to a free surface of a polymer film penetrate much deeper for dynamical than for structural properties [11, 12, 30]. However, different penetration depths for different dynamical measurements of relevance would be unexpected and have not been identified in our knowledge.

In this work, we perform large-scale MD simulations of polymer films at equilibrium at an exceptionally low temperature and a zero pressure using GPU-based brute-force computing with individual runs executed for 5 months. Comprehensive measurements on depth-dependent structural and dynamical properties are performed. Surface enhanced dynamics is exemplified in particular by a higher particle hopping rate close to the surface. Unexpectedly, the surface enhancement on the hopping rate terminates abruptly when going deeper into the film. This is similar for other hop related dynamical measurements at short time scales. In contrast, surface effects on other dynamical measurements at longer time scales show much deeper penetrations. They include particle mobility measured at longer time scales and hopping event correlations quantifying dynamic heterogeneity. There thus exists a region in which the particle hopping rate is bulk-like but the particle mobility and dynamic heterogeneity are surface affected. This is a unique example in which one can perturb certain dynamic quantities relevant to structural relaxations while maintaining other dynamic quantities unchanged.

The rest of the paper is organized as follows. Section II introduces the model and the simulation methods. Sections III and IV present results on structural and dynamical properties, which motivate the definition of three sublayers of the surface mobile layer. We then discuss in Sec. V detailed properties and possible origins of the sublayers. Implications of our findings on theoretical understanding of glass is discussed in Sec. VI. Finally,

* Email: C.H.Lam@polyu.edu.hk

Sec. VII concludes the paper with a summary and some further discussions.

II. MODEL AND SIMULATION METHODS

Our simulations are based on the Kremer-Grest model of bead-spring polymer widely used in the literature [11, 12, 29–38]. We adopt the variant used in Ref. [38] in which polymer chains possess heavier chain-tails so that all monomers have similar mobilities. Specifically, we simulate polymer melts consisting of chains which are 10 monomers long. This is well below the entanglement chain length [39] and it thus models unentangled short-chain polymer following Rouse dynamics [40]. We refer to the monomers as particles. Pairs of particles interact via the Lennard Jones (LJ) potential $4\epsilon \left[(\sigma/r)^{12} - (\sigma/r)^6 \right]$ with an interaction cutoff distance $R_c = 2 \cdot 2^{1/6} \sigma \simeq 2.24\sigma$ beyond which it becomes a constant. Besides short-range repulsion, the potential implements longer-range attraction which is essential for simulating polymer films with free surfaces. Bonded particles are further bounded by a finitely extensible nonlinear elastic (FENE) potential $-\frac{k}{2} R_0^2 \ln \left[1 - (r/R_0)^2 \right]$ where $k = 30\epsilon/\sigma^2$ and $R_0 = 1.5\sigma$. We adopt dimensionless LJ units which amounts to taking $\sigma = \epsilon = 1$. Internal particles in each chain have a mass $M_I = 1$. The heavier chain-tail property amounts to assigning a larger mass $M_T = 4$ to the particles at both ends of each chain. This leads to an approximately uniform mobility for all particles as indicated by particle mean squared displacements (MSD). Throughout the paper, we express lengths in unit of σ for clarity even though $\sigma \equiv 1$.

Simulations are performed in a box of dimensions $L \times L \times \infty$ with $L = 24\sigma$ following periodic boundary conditions in the x and y directions. We consider free-standing polymer films each having 1200 chains leading to totally 12000 particles. This provides free surfaces on both sides. Centering the film at $z = 0$, results presented for $z \geq 0$ in general are averages over the $\pm z$ positions.

Our main results are measured from films fully equilibrated at temperature $T = 0.36$, which is about the lowest temperature for practical equilibrium simulation of the model with existing computing technologies. The pressure is zero since empty regions exist above and below the film. All simulations are performed using the HOOMD software package [41] under NVT conditions with a time step of 0.005. The chain configurations in the films are initialized randomly and thermalized at $T = 0.8$ following standard techniques [32, 34]. They are subsequently annealed at $T = 0.5$ and then repeatedly cooled and annealed by temperature steps of $\Delta T = 0.02$. Individual cooling and annealing processes both involve 10^7 timesteps. At the final $T = 0.36$, each film is further annealed for 10^{10} timesteps before data taking. This procedure has been found to generate well-equilibrated polymer melts in bulk simulations with particle MSD

exceeding $5.0\sigma^2$ [38]. The equilibration takes about 5 months using a nVidia GTX580 GPU.

We prepare 5 independent film samples using the procedures above. For each sample, we perform 3 data collection runs at $T = 0.36$ each of 8×10^7 timesteps. To enhance the statistics, these data collection runs are separated by further annealing of 10^9 timesteps during which data are not collected. All our quantitative measurements are averaged over both surfaces in these 15 data collection runs. Errors are estimated from fluctuations among the 5 independent film samples. The computations involved in this study are in our knowledge the most intensive ones for bead-spring polymer films reported in the literature.

All our analysis are based on coarse-grained particle trajectories $\mathbf{r}_i(t)$ recorded during data collection runs. Here, each value of $\mathbf{r}_i(t)$ is a coarse-grained position of particle i defined by

$$\mathbf{r}_i(t) = \langle \mathbf{r}_i^0(t') \rangle_{t' \in [t, t + \Delta t_c]} \quad (1)$$

where $\mathbf{r}_i^0(t)$ denotes its instantaneous position. The averaging duration $\Delta t_c = 5$ is chosen to be well in between the typical particle vibrational oscillation period and the waiting time between two consecutive hops of a particle. Therefore, $\mathbf{r}_i(t)$ nearly always points to a meta-stable particle position, rather than somewhere interpolating between two meta-stable positions related by a hop. In each data collection run, we record coarse-grained trajectories in the form of 2×10^4 snapshots of coarse-grained positions $\mathbf{r}_i(t)$ taken after every 4000 timesteps corresponding to a duration of $\tau_{min} = 20$.

III. STATIC STRUCTURAL PROPERTIES

Figure 1 plots the particle density ρ of the film as a function of the non-planar coordinate z . It shows that ρ converges to its bulk value at a very shallow depth from the free surface as observed in previous works [12, 30]. It is well fitted by [30]

$$\rho = \frac{\rho_0}{2} \text{Erfc} \left(\frac{z - h_0}{\sqrt{2}\sigma_h} \right) \quad (2)$$

appropriate for surfaces limited by surface tension [42], where Erfc is the complementary error function. From the fit, we find a bulk particle density $\rho_0 = 1.04$, a half film thickness $h_0 = 9.99\sigma$ and a surface width $\sigma_h = 0.248\sigma$. Figure 1 also shows spatial density oscillations of a small amplitude close to the surface. This corresponds to slight layering effects and only occurs to our samples at very low T after long annealing. These small modulations however appear to have negligible impacts on other properties to be discussed.

To define further layer-resolved quantities, let Ω_z be a layer of particles in between $z \pm \Delta z/2$. In all following quantitative measurements, we consider a layer thickness $\Delta z = 0.5$. For any 3D position \mathbf{r} , the projection onto

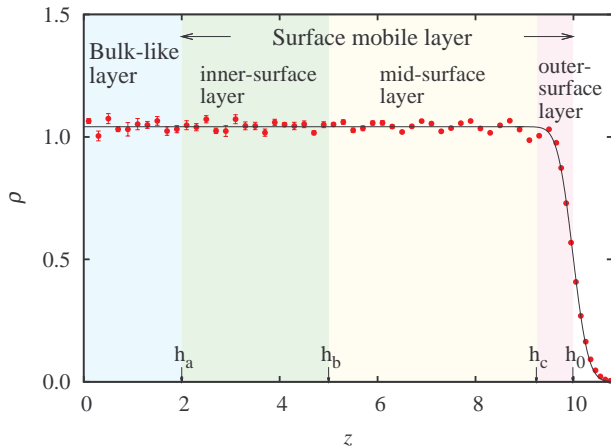


FIG. 1. (a) Particle density ρ against coordinate z for free-standing films centered at $z = 0$. The solid curve represents a fit to Eq. (2). The position $z = h_0 \equiv 9.99\sigma$, where $\sigma \equiv 1$, marks the average position of the film surface, with h_0 being the half film thickness. The surface mobile layer consists of the outer-, mid- and inner-surface layers, which are bounded below respectively by $h_a \equiv 2.0\sigma$, $h_b \equiv 5.0\sigma$ and $h_c \equiv 9.25\sigma$.

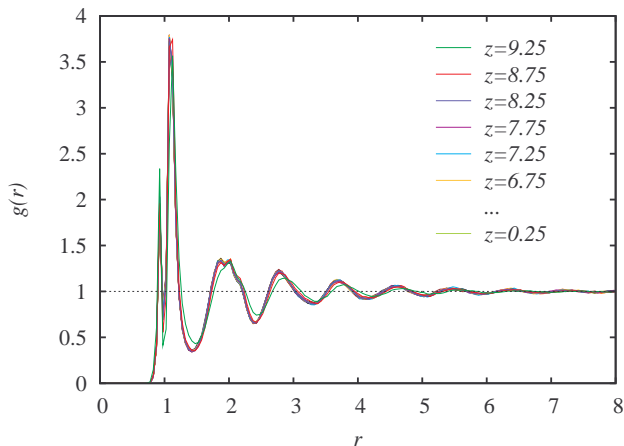


FIG. 2. (a) 2D pair distribution function of particles $g(r)$ against 2D distance r defined on the xy plane. All curves collapse apart from some slight deviations for $z = 9.25\sigma$.

the xy -plane is denoted by $\tilde{\mathbf{r}}$, and it is similar for other position vectors. The 2D local particle density $\tilde{\rho}(\tilde{\mathbf{r}})$ of layer Ω_z at 2D position $\tilde{\mathbf{r}}$ is then

$$\tilde{\rho}(\tilde{\mathbf{r}}) = \sum_{i \in \Omega_z} \delta^2(\tilde{\mathbf{r}} - \tilde{\mathbf{r}}_i) \quad (3)$$

where δ^2 denotes the 2D Dirac delta function. The 3D particle density ρ shown in Fig. 1 relates to $\tilde{\rho}$ by $\rho = \langle \tilde{\rho}(\tilde{\mathbf{r}}_0) \rangle / \Delta z$, where the average is taken over all 2D positions $\tilde{\mathbf{r}}_0$.

The 2D pair distribution function of particles in layer

Ω_z can now be defined as

$$g(r) = \frac{\langle \tilde{\rho}(\tilde{\mathbf{r}}_0) \tilde{\rho}(\tilde{\mathbf{r}}_0 + \tilde{\mathbf{r}}) \rangle}{\langle \tilde{\rho}(\tilde{\mathbf{r}}_0) \rangle^2} \quad (4)$$

where $r = |\tilde{\mathbf{r}}|$ and averages are performed over 2D positions $\tilde{\mathbf{r}}_0$. In practice, it is evaluated using the equivalent form [43]

$$g(r) = \frac{1}{\pi r L^2 \langle \tilde{\rho}(\tilde{\mathbf{r}}_0) \rangle^2} \left\langle \sum_{\substack{i,j \in \Omega_z \\ (i>j)}} \delta^2(\tilde{\mathbf{r}} - |\tilde{\mathbf{r}}_i - \tilde{\mathbf{r}}_j|) \right\rangle. \quad (5)$$

Figure 2 plots $g(r)$ against r for various layer positions z . The main peak at $r \simeq \sigma$ is split into two subpeaks corresponding to bonded and non-bonded nearest neighbors, while the weaker peaks are due to further neighbors. Moreover, $g(\tilde{\mathbf{r}})$ for $z \lesssim 9.25\sigma$ are practically independent of z , representing the bulk values. Deviations dramatically increase only for $z \gtrsim 9.75\sigma$ (data not shown).

Therefore, both ρ and $g(r)$ exhibit bulk-like values except at very close to the free surface. Surface effects on structural measurements studied are significant only for $z \geq h_c \equiv h_0 - 3\sigma_h = 9.25\sigma$ and we refer to the region as the outer-surface layer (see Fig. 1).

IV. DYNAMICAL PROPERTIES

A. Displacement statistics

Let Δr_i be the displacement of particle i over a duration τ at time t_0 defined by

$$\Delta r_i = |\mathbf{r}_i(t_0 + \tau) - \mathbf{r}_i(t_0)|, \quad (6)$$

which is a net displacement in general shorter than the distance traveled along the actual path. The particle MSD at layer Ω_z is then given by

$$\text{MSD} = \langle \Delta r_i^2 \rangle_{i \in \Omega_z} \quad (7)$$

where the average is limited to particles in the layer Ω_z . Particle i is deemed inside Ω_z if its position $\mathbf{r}_i(t_0)$ at the initial time t_0 of the displacement is within the layer. Since we focus on the small displacement regime, adopting other more stringent criteria [12] does not alter our results qualitatively and this is further discussed in Appendix A.

Figure 3(a) plots the measured MSD against the duration τ for various layer positions z . The layer thickness used is $\Delta z = 0.5$ but we have performed averaging over every two neighboring layers to thin out the data for clarity. Results are qualitatively similar to those in Ref. [12]. For $z \lesssim 2.5$, the MSD is approximately independent of z representing the bulk values. In contrast, for $z \gtrsim 3.5\sigma$, it increases dramatically with z , demonstrating surface enhanced dynamics. This also shows that surface effects penetrate far beyond the outer-surface layer and extend

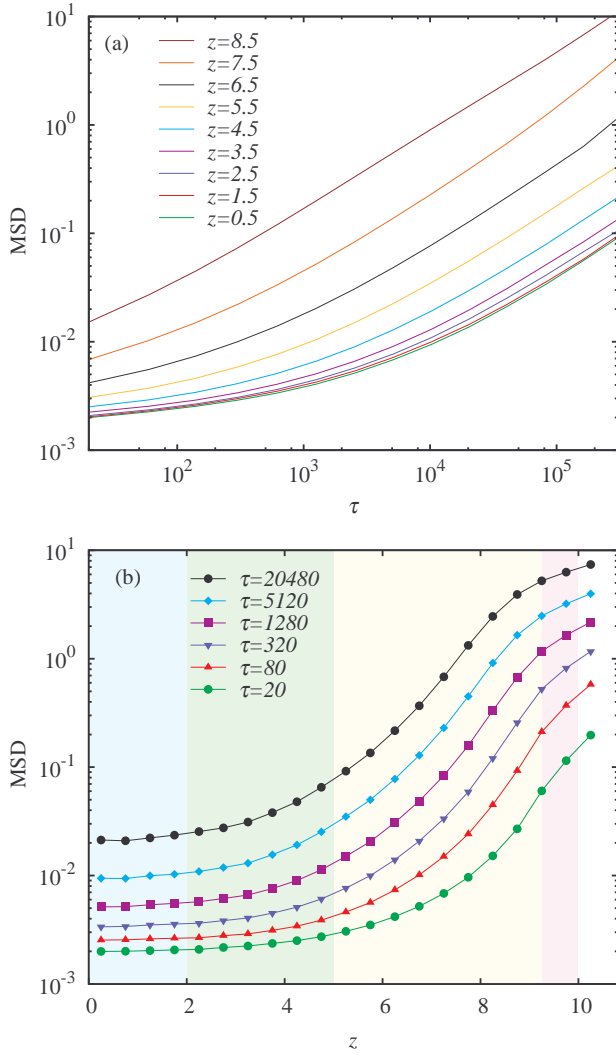


FIG. 3. (a) Particle mean square displacement (MSD) against duration τ for $z = 0.5\sigma, 1.5\sigma, \dots$ (from bottom to top) where $\sigma \equiv 1$. The MSD increases dramatically with z for $z \gtrsim 3.5\sigma$ indicating surface enhanced mobility. (b) MSD against coordinate z plotted using the same data as in (a).

much deeper than those on the structural properties as observed previously [12]. This is more clearly observed in Figure 3(b) which replots the MSD against z for various duration τ . It is also evident that surface effects penetrate deeper as τ increases.

We next study the probability distribution $P(\Delta r)$ followed by the displacement Δr_i , which is closely related to the van Hove self-correlation function [44]. Figure 4(a) plots the computed $P(\Delta r)$ at $z = 0.25\sigma$ deep in the bulk-like region for various duration τ . The results are similar to those from bulk simulations of the same model in Ref. [38]. Besides a main peak, a secondary peak at $\Delta r \simeq 0.9\sigma$ emerges as τ increases and corresponds to particle hops. The activated nature of hopping is evidenced by a dip in $P(\Delta r)$ at $\Delta r \simeq 0.6\sigma$.

Besides hops, let us refer to all other non-vibrational

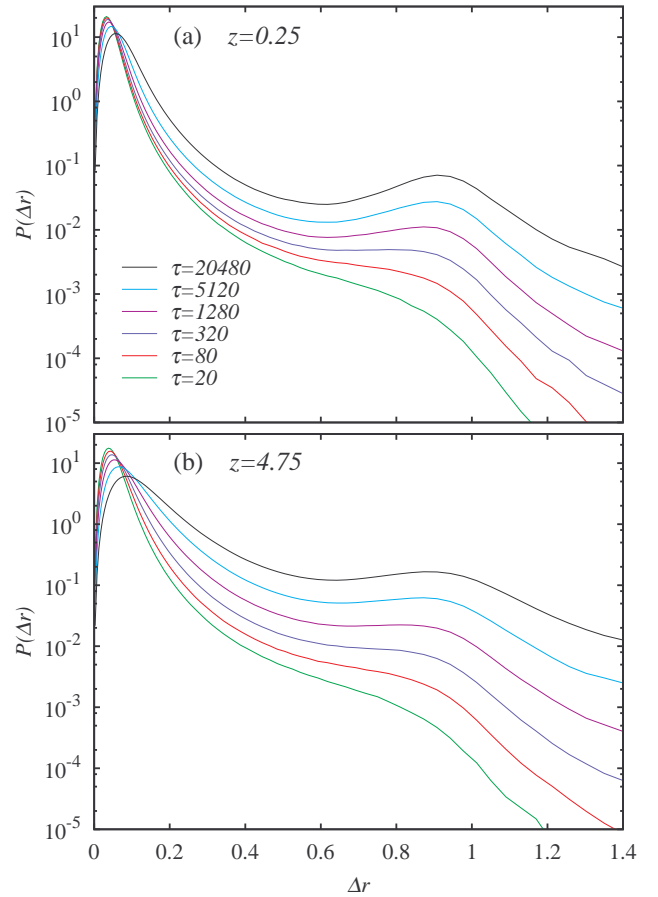


FIG. 4. Probability distribution $P(\Delta r)$ of particle displacement Δr over duration τ at $z = 0.25\sigma$ in the bulk-like layer (a) and at $z = 4.75\sigma$ in the inner-surface layer (b). In both cases, the main peak at $z \simeq 0$ corresponds to particles which have not hopped and its broadening at increasing τ is due to particle creep motions. The secondary peak at $z \simeq 0.9\sigma$ is due to particle hops. The dip at $z \simeq 0.6\sigma$ is adopted as the threshold of hopping.

motions mainly due to accumulation of smaller displacements as particle creep motions. At small duration τ , a displacement $\Delta r > 0.6\sigma$ thus usually results from a hop while $\Delta r < 0.6\sigma$ usually implies vibrations or creep motions. From Fig. 4(a), as τ increases from 20 to 80, $P(\Delta r)$ at $\Delta r \simeq 0.9\sigma$ increases considerably and indicates significant hopping motions. The main peak however broadens only slightly implying that creep motions are negligible.

Figure 4(b) shows another example of $P(\Delta r)$ at $z = 4.75\sigma$ which admits some mild surface enhanced dynamics as indicated by the MSD in Fig. 3(a). This choice of z will be more apparent later. Results in Fig. 4(b) are similar to those in Fig. 4(a) except that as τ increases from 20 to 80, the broadening of the main peak is much more significant. This indicates that the surface enhanced dynamics at $z = 4.75\sigma$ are contributed significantly by enhanced creep motions.

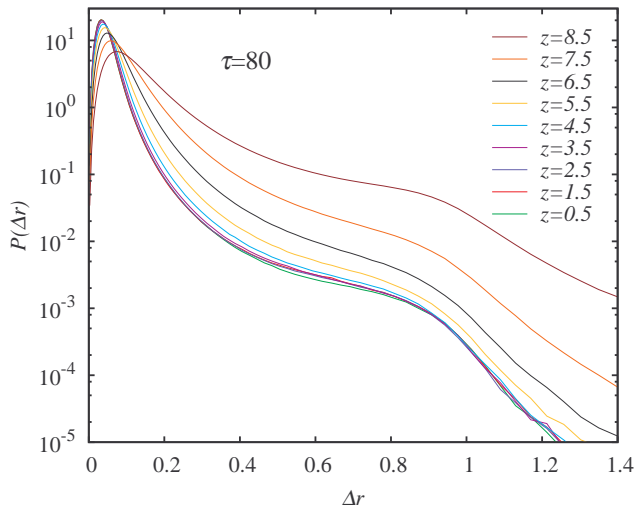


FIG. 5. Probability distribution $P(\Delta r)$ of particle displacement Δr over a short duration $\tau = 80$. At $z = 4.5\sigma$, it begins to deviate noticeably from its bulk value signifying the onset of surface enhanced motions. The deviation is proportionately more prominent at $\Delta r \simeq 0.2\sigma$ than at 0.9σ , implying a stronger enhancement on particle creep motions than on hops.

To better compare between the layers, Fig. 5 plots $P(\Delta r)$ at $\tau = 80$ for various z . For $z \geq 5.5\sigma$, $P(\Delta r)$ is beyond the bulk value for all Δr . At $z = 4.5\sigma$ close to the onset of surface effects, $P(\Delta r)$ is slightly but distinctly beyond the bulk value for $\Delta r \simeq 0.3\sigma$ indicating broadening of the main peak. However, it is indistinguishable from the bulk value at $\Delta r \simeq 0.9\sigma$ showing no growth of the secondary peak. This hence shows that the surface effects reach as deep as $z = 4.5\sigma$ for creep motions but not for hops. An explanation of this observation will be discussed in Sec. V.

B. Particle hopping rates

We considered particle i as having hopped during a period τ if its displacement Δr_i defined in Eq. (6) satisfies

$$\Delta r_i \geq 0.6\sigma \quad (8)$$

following Ref. [38], where the threshold 0.6σ is the position of the first dip in $P(\Delta r)$ from Fig. 4(a). The net hopping rate $R(\tau)$ can be defined as

$$R(\tau) = \frac{1}{\tau} \langle \theta(\Delta r_i - 0.6\sigma) \rangle_{i \in \Omega_z} \quad (9)$$

where θ denotes the Heaviside step function. This provides a net hopping rate because Δr_i defined in Eq. (6) is a net displacement so that round trips, for example, do not contribute.

Figure 6 shows the main result of this work which is a plot of the computed $R(\tau)$ against z for various duration

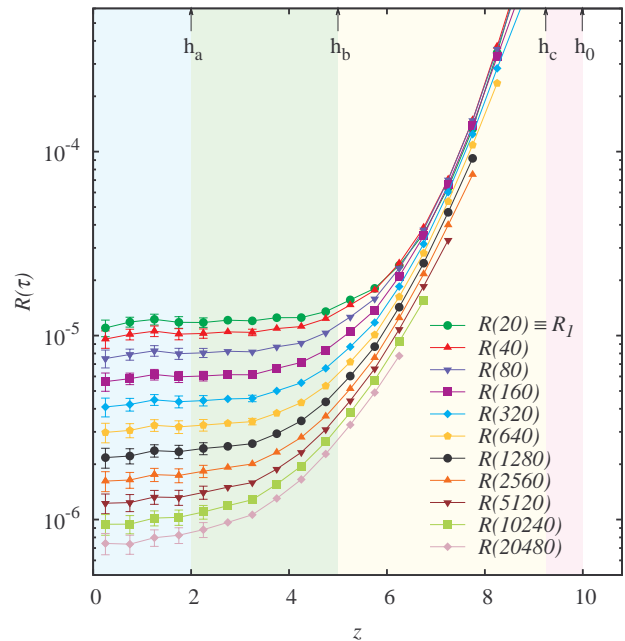


FIG. 6. Particle net hopping rate $R(\tau)$ against coordinate z based on net displacement over duration τ . Particle hopping rate R_1 is identified as $R(\tau_{min})$ where $\tau_{min} = 20$. Since R_1 converges to its bulk value quite abruptly at $z \simeq h_b \equiv 5\sigma$, surface effects on R_1 do not reach the inner surface layer. In contrast, $R(\tau)$ at larger τ converges only deeper into the film, indicating that their surface effects penetrate into the inner surface layer as well. Errorbars smaller than the symbols are omitted.

τ . We have included only data satisfying $\tau R(\tau) \leq 0.2$, a typical constraint for simple rate measurement. We have also checked that the displacement distribution $P(\Delta r)$ corresponding to each data point exhibits a clear secondary bump or peak at 0.9σ so that particle hops indeed dominate. From Fig. 6, $R(\tau)$ decreases dramatically with τ in general. Detailed examinations of individual particle trajectories show that this is due to the abundance of back-and-forth hopping motions at low T widely studied in the literature [38, 45–52]. Since $R(\tau)$ is a net hopping rate not registering the back-and-forth parts of the hops, at large τ , it underestimates the true hopping rate and is instead a better indicator of particle mobility describing long-time motions in the diffusive regime. Now, we approximate the true hopping rate R_1 using the net rate $R(\tau)$ at the smallest studied τ , i.e.

$$R_1 = R(\tau_{min}) \quad (10)$$

where $\tau_{min} \equiv 20$. Since τ_{min} must also be much longer than the duration of the course of a hop, called the instanton time [53], the current value should already be about the smallest practical one.

A main observation in this work is that R_1 in Fig. 6 converges rather abruptly to its bulk value exhibiting a surprisingly wide plateau which begins to curve up only

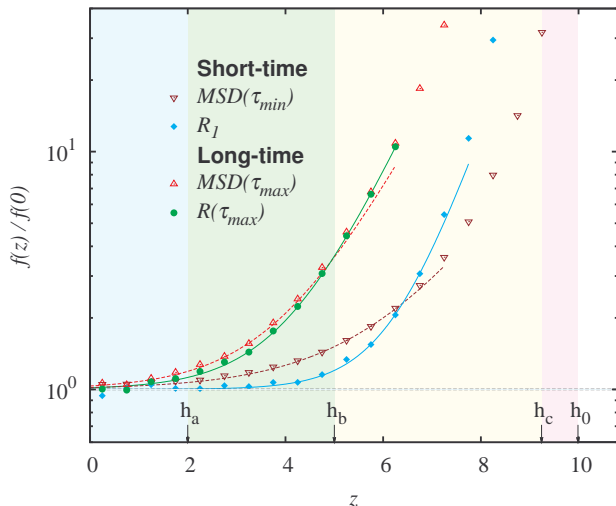


FIG. 7. Layer-resolved quantity $f(z)$ normalized with respect to bulk value $f(0)$ against coordinate z . Quantities considered are the MSD and the particle hopping rate R_1 defined at short time $\tau_{min} = 20$, as well as the MSD and the net hopping rate $R(\tau_{max})$ at long time $\tau_{max} = 20480$. The solid lines show fitted curves using Eq. (17).

not far away from the free surface. This is in contrast to the case of the MSD for the same duration τ_{min} shown in Fig. 3(b). Figure 6 also shows that surface effects on $R(\tau)$ penetrates deeper as τ increases, analogous to that revealed by the MSD.

Figure 7 shows on the same plot both the MSD and $R(\tau)$ at τ being $\tau_{min} \equiv 20$ and $\tau_{max} \equiv 20400$ normalized by the respective bulk values. For τ_{min} , it is clear that $R_1 \equiv R(\tau_{min})$ converges to its bulk value much more abruptly than the MSD. For τ_{max} related to particle mobility, the normalized MSD and $R(\tau_{max})$ are close to each other. Fits of these quantities to an exponential functional form will be explained in Sec. V.

From Fig. 7, since surface effects on R_1 are small at $z < h_b$ where $h_b = 5.0\sigma$, we refer to the region $h_b \leq z \leq h_c$ as the mid-surface layer (see Fig. 1). This sublayer is characterized by a surface enhanced R_1 despite bulk-like structural properties. Similarly, surface effects on $R(\tau_{max})$ are negligible for $z < h_a$ where $h_a = 2.0\sigma$ and we define the inner-surface layer as the region $h_a \leq z \leq h_b$ (see also Fig. 1). It is characterized by a surface enhanced $R(\tau_{max})$ despite a bulk-like R_1 . Note that a larger τ_{max} may increase h_a , but should not affect our conclusions qualitatively.

C. Dynamic heterogeneity

Particle motions in glassy systems are known to exhibit strong spatial-temporal correlations in the form of dynamic heterogeneity [54]. The surface mobile layer is expected to show reduced dynamic heterogeneity because

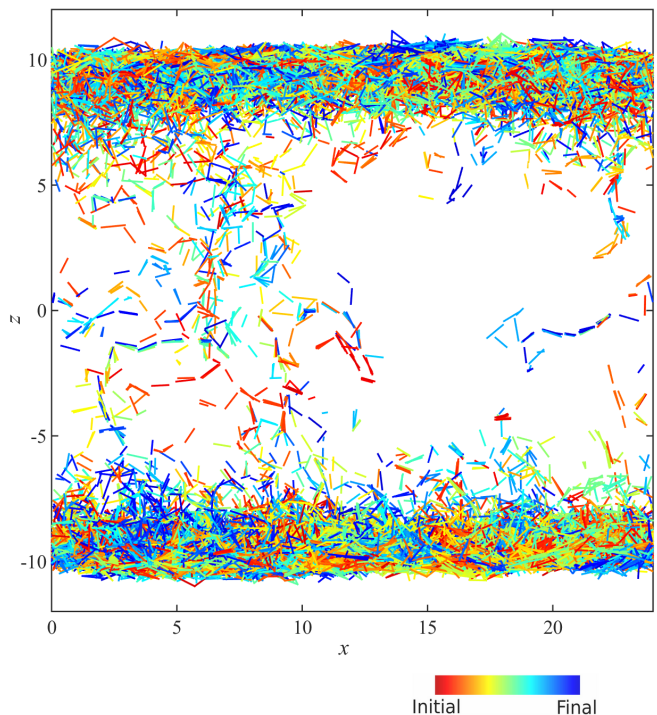


FIG. 8. Hopping events as illustrated by coarse-grained particle trajectories during hopping in a typical film. A particle generates a hopping event if its displacement during any time interval $\tau_{min} = 20$ is beyond 0.6σ . The diagram shows all hopping events occurring over a period $\tau = 10,000$. Color represents time at which the hop occurs relative to the duration τ , as indicated in the legend. The high density of hopping events on both the upper and lower surfaces of the free standing film illustrates enhanced surface mobility. Closer to the center of the film, events are fewer and string-like motions and their repetitions can be observed. Dynamic heterogeneity is also revealed from the spatial distribution of these dynamical events.

of its Arrhenius dynamics characteristic of non-glassy liquids [13]. In this section, we show qualitatively that surface effects reducing the dynamic heterogeneity penetrate into the inner-surface layer. Quantitative analysis will be presented in the next section.

Discretizing time by defining $t_k = k\tau_{min}$. The displacement Δr_i^k of particle i at time t_k during τ_{min} is defined by

$$\Delta r_i^k = |\mathbf{r}_i(t_{k+1}) - \mathbf{r}_i(t_k)|, \quad (11)$$

which is the short-time particular case of Eq. (6). Particle i is considered as having hopped at time t_k if $\Delta r_i^k \geq 0.6\sigma$. Figure 8 shows all hopping events in the film during $0 \leq t_k < \tau$ where $\tau = 10,000$. Specifically, if particle i hops at time t_k , its trajectory during the hop is illustrated by a line segment joining $\mathbf{r}_i(t_k)$ and $\mathbf{r}_i(t_{k+1})$. Non-hopping parts of the trajectories are omitted. Trajectories are colored based on the value t_k/τ , so that hops at similar times are shaded in similar colors.

We observe from Fig. 8 that hopping events are much

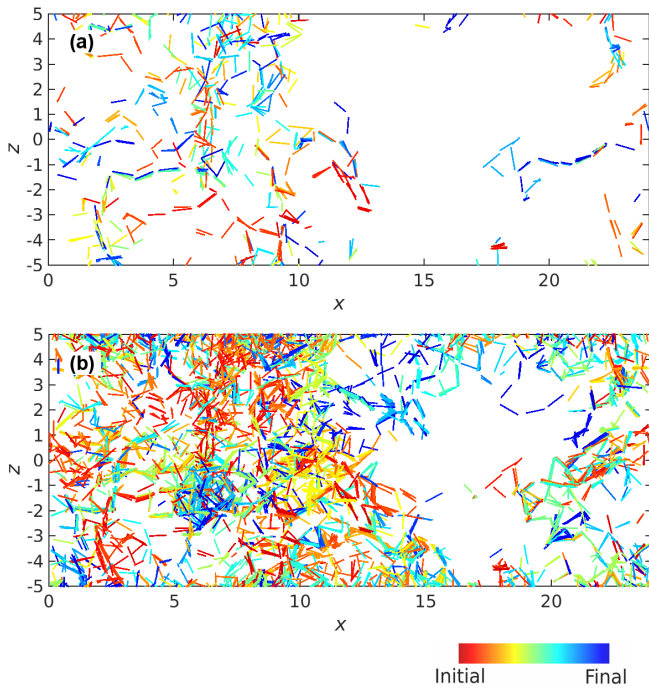


FIG. 9. (a) Hopping events from Fig. 8 but limited only to the bulk-like and inner-surface layers at $|z| \leq 5.0\sigma$ both following the bulk-like hopping rate R_1 . Events occurring over a period $\tau = 10,000$ are shown. (b) The period is extended to $\tau = 100,000$ for the same polymer sample. A stronger dynamic heterogeneity is observed closer to the center than at the margins of the region, although the density of the hopping events is statistically uniform. This visually illustrates the co-existence of a z -independent average particle hopping rate and a z -dependent dynamic heterogeneity. A similar but weaker trend concerning the dynamic heterogeneity can also be observed in (a).

more numerous close to the surface. This illustrates enhanced surface mobility ultimately resulting from the reduced particle coordination at the surface. Beneath the surfaces where individual hopping events can be resolved, we observe many string-like motions [55] each corresponding to multiple particle trajectories lining up to form a nearly continuous curve typically punctuated by tiny gaps. A closer look can also reveal reversals and repetitions of strings corresponding to particle back-and-forth hopping motions, as indicated by one string closely retracing another one [38].

Enhanced mobility propagates into the film via string-like motions originating from close to the free surfaces. The spatial extent of string-like motions thus provides a minimum length scale characterizing the depth variation of the particle hopping rate. The density of hopping events in Fig. 8 is proportional to R_1 and decreases monotonically with $|z|$. Focusing on the region in which R_1 and the hopping event density have converged to their bulk values, Fig. 9(a) replots the same hopping events from Fig. 8 but limited to the inner-surface and the bulk-like layers at $|z| \leq 5\sigma$. Similarly, Fig. 9(b) shows additional

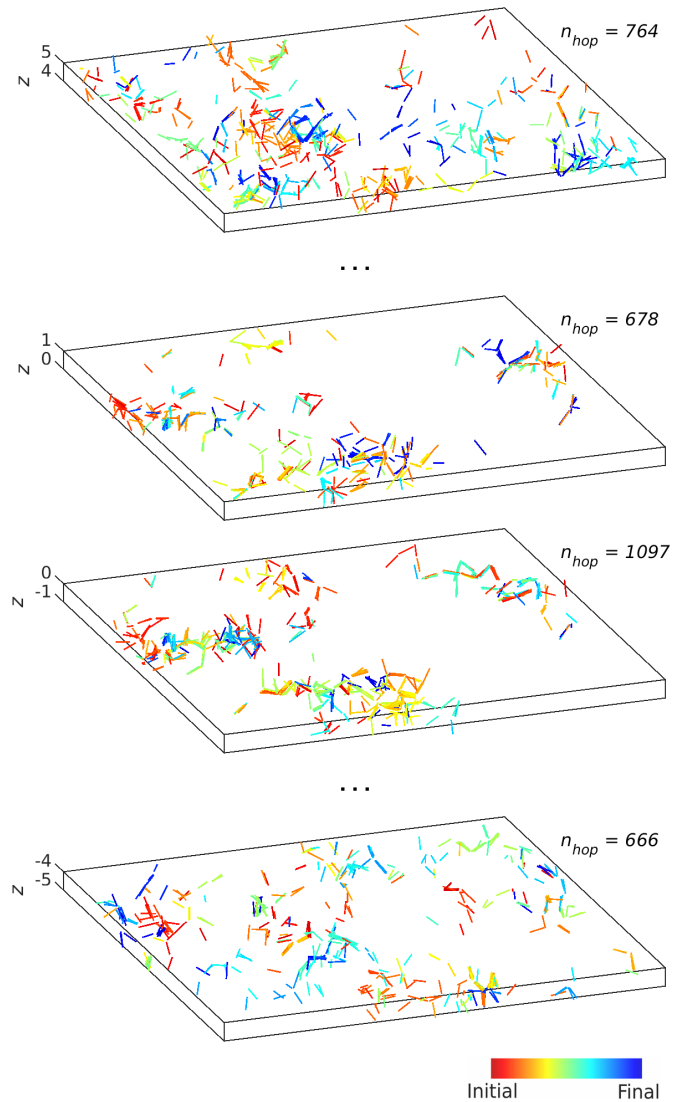


FIG. 10. 3D views of hopping events in individual layers from Fig. 9(b) each of thickness σ . Stronger dynamic heterogeneity is observed at $|z| \in [0, \sigma]$ (middle layers) than at $|z| \in [4\sigma, 5\sigma]$ (top and bottom layers), although the numbers of hops n_{hop} are similar as dictated by the uniform bulk-like hopping rate R_1 .

hopping events in the same region by extending the imaged period to $\tau = 100,000$. Dynamic heterogeneity is readily observed and is depicted mainly as concentrations of hopping events in between relatively empty regions. It can also be observed via temporal correlations of the hops as revealed by correlations in the colors of the trajectories. It is evident from Fig. 9(b) that surface effects reducing the dynamic heterogeneity penetrate into the inner-surface layer. This is in sharp contrast to R_1 which exhibits no surface effect in this layer. Similar trends are also barely discernible in Figure 9(a) despite stronger statistical fluctuations.

The hopping events in Fig. 9(b) are resolved into layers according to the position $\mathbf{r}_i(t_k)$ at the beginning of

a hop. Four examples of these layers are shown in Figure 10. The numbers of hopping events n_{hop} in the layers are also shown, which are basically uniform apart from statistical fluctuations. We observe stronger concentrations of events at $z = \pm 0.5\sigma$ at the film center. In contrast, events at $z = \pm 4.5\sigma$ are clearly more homogeneously distributed, indicating reduced heterogeneity. Surface effects on dynamic heterogeneity thus evidently extends into the inner-surface layer.

D. Hopping event correlations

We now further analyze the dynamic heterogeneity quantitatively. We represent the location of a hopping event by the mean position

$$\mathbf{r}_i^k = \frac{1}{2}(\mathbf{r}_i(t_k) + \mathbf{r}_i(t_{k+1})). \quad (12)$$

The 2D local hopping event density in layer Ω_z during time τ is given by

$$\rho^H(\tilde{\mathbf{r}}, \tau) = \sum_{k=1}^{\tau/\tau_{min}} \sum_{i \in \Omega_z} \theta(\Delta r_i^k - 0.6\sigma) \delta^2(\tilde{\mathbf{r}} - \tilde{\mathbf{r}}_i^k) \quad (13)$$

where $\tilde{\mathbf{r}}_i^k$ denotes the projection of \mathbf{r}_i^k onto the xy -plane. Furthermore, the 2D pair distribution function of hopping events can be defined, analogous to Eq. (4), by

$$g^H(r, \tau) = \frac{\langle \rho^H(\tilde{\mathbf{r}}_0, \tau) \rho^H(\tilde{\mathbf{r}}_0 + \tilde{\mathbf{r}}, \tau) \rangle}{\langle \rho^H(\tilde{\mathbf{r}}_0, \tau) \rangle^2} \quad (14)$$

where $r = |\tilde{\mathbf{r}}|$ and the averages are over all 2D positions $\tilde{\mathbf{r}}_0$. It is numerically evaluated using a form analogous to Eq. (5).

Figure 11(a) plots $g^H(r, \tau)$ against r for $\tau = 20$ (i.e. τ_{min}). It involves only a single snapshot of hopping events and $g^H(r, \tau)$ is simply a layer-resolved pair distribution function of the most mobile particles. Peaks are observed at $r \simeq 0.9\sigma$, 1.7σ , etc., similar to previous studies for bulk systems [56]. They correspond to nearest, next nearest neighbors, etc., within string-like motions. Figure 11(b)-(c) shows $g^H(r, \tau)$ for $\tau = 40$ and 20480 (i.e. τ_{max}) respectively. A prominent main peak at $r = 0$ is also observed. It indicates abundance of multiple hops at the same position at different times t_k and are mainly due to back-and-forth hopping motions.

We observe from Fig. 11(a)-(c) that $g^H(r, \tau)$ is reduced close to the surface. Surface effects penetrate up to $z \simeq 5.5\sigma$ for $\tau = 20$ and 40, but reach deeper to $z \simeq 4.5\sigma$ for $\tau = \tau_{max}$. To establish this more clearly, we numerically evaluate an integrated hopping event correlation defined by

$$G^H(\tau) = 2\pi \int_0^{4\sigma} r (g^H(r, \tau) - 1) dr \quad (15)$$

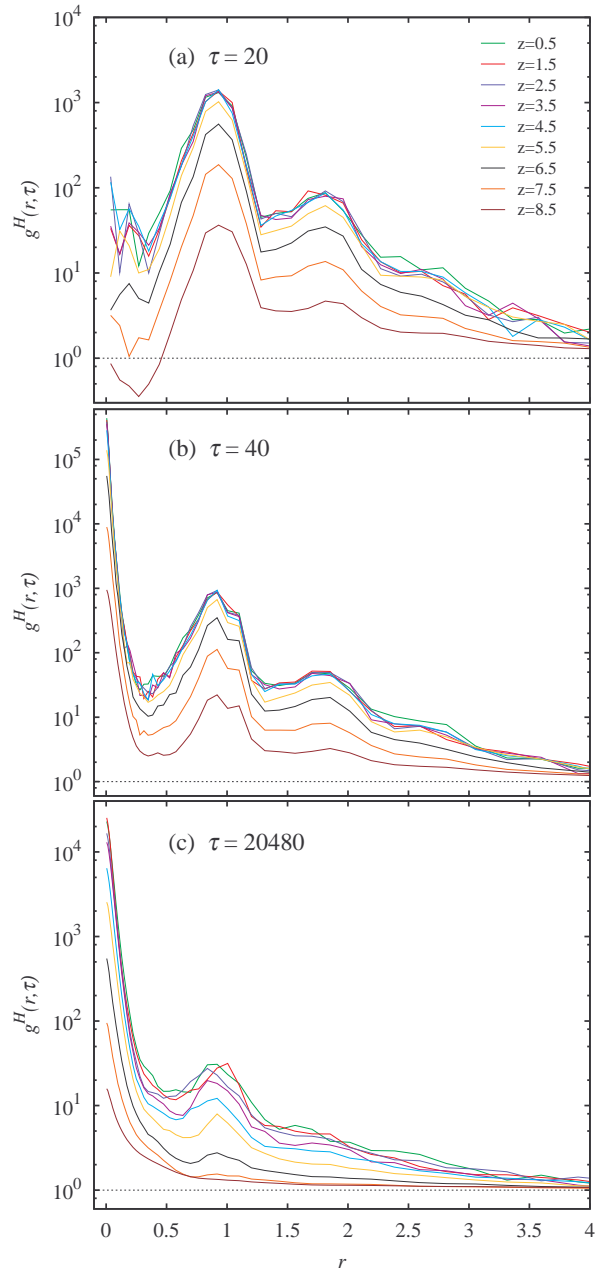


FIG. 11. Hopping event pair distribution function $g^H(r, \tau)$ for hops occurring over a duration $\tau = 20$ (a), 40 (b) and 20480 (c). Hops are defined based on displacements during a time $\tau_{min} = 20$. As z increases, $g^H(r, \tau)$ decreases and this shows surface induced reduction of dynamic heterogeneity. Surface effects have practically terminated at $z = 4.5\sigma$ in (a) and (b) but only at $z = 2.5\sigma$ in (c).

motivated by $g^H(r, \tau) = 1$ as $r \rightarrow \infty$. Results are plotted in Fig. 12 which further show that surface effects penetrate deeper as τ increases. In Eq. (15), the integration upper bound is taken as 4σ to include a large regime where $g^H(r, \tau) \gg 1$ for better statistics, but other values give qualitatively similar results.

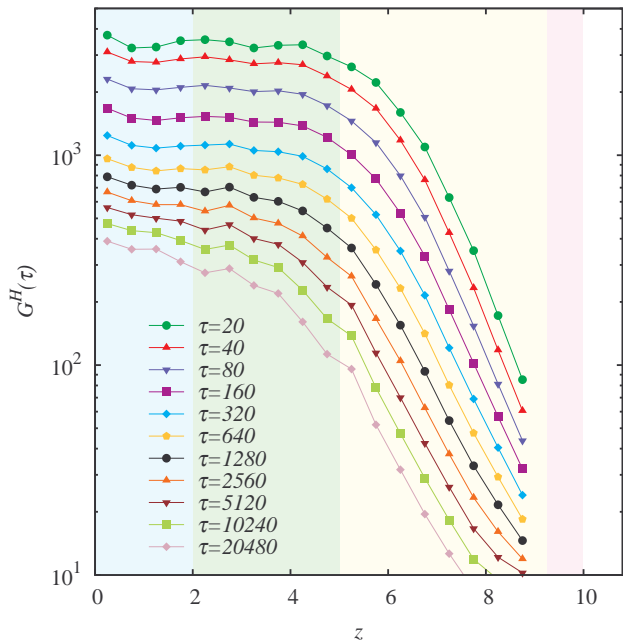


FIG. 12. Correlation $G^H(\tau)$ for hopping events occurring over a duration τ .

Particle back-and-forth motions have long been studied in glassy systems [38, 45–52] and cause the main peak at $r = 0$ in Fig. 11(b)-(c). We now analyze them by generalizing the approach in Ref. [38] to layer-resolved measurements. Specifically, after particle i in layer Ω_z has hopped at time t_k , we define its further motion as a returning hop if it first returns to within a distance 0.3σ from the original position $\mathbf{r}(t_k)$. Alternatively, the motion is defined as a non-returning second hop, i.e. an escaping hop, if it first displaces again elsewhere beyond a distance 0.6σ from the hopped position $\mathbf{r}(t_{k+1})$. We monitor the particle up to time $t_k + 2 \times 10^5$ which is long enough so that the subsequent motions can be categorized in most cases. We hence calculate the probabilities P_{ret} and P_2 that the particle first performs a returning or a non-returning second hop respectively. Results are shown in Fig. 13(a). We observe that in the bulk-like layer, $P_{ret} \simeq 0.86$ which is a very high value implying a surprisingly strong temporal anti-correlation in the hopping of individual particles. In the mobile layer, P_{ret} decreases monotonically towards the free surface. At the outer-surface layer, the much smaller value of $P_{ret} \simeq 0.30$ is consistent with simple uncorrelated motions as is expected from the non-glassy nature of the surface layer [13]. Note that the value 0.86 in the bulk is larger than 0.73 obtained in Ref. [38] from bulk simulations because significantly more detailed trajectories with positions recorded every period $\tau_{min} \equiv 20$ are used here so that most instances of back-and-forth motions are captured in the analysis.

We next calculate the rates R_{ret} and R_2 of returning

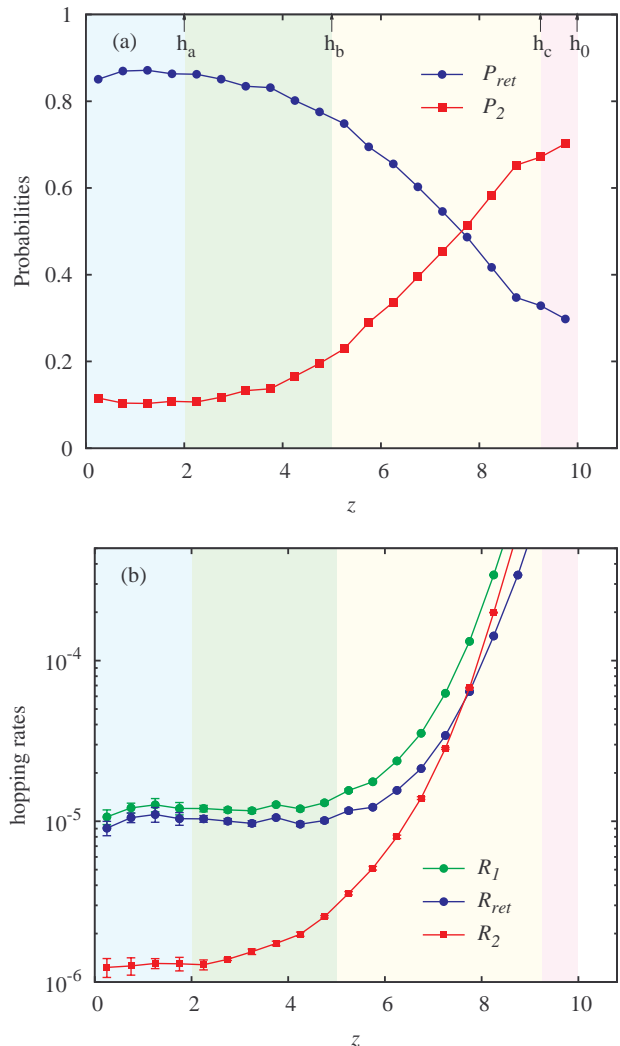


FIG. 13. Probabilities P_{ret} and P_2 (a) of returning and non-returning second hops and the corresponding rates R_{ret} and R_2 (b) against coordinate z . The hopping rate R_1 is also shown in (b).

and non-returning second hops using

$$R_{ret} = R_1 P_{ret} \quad \text{and} \quad R_2 = R_1 P_2. \quad (16)$$

where R_1 as defined in Eq. (10) can be interpreted as the rate of the first hop, noting that every hopping event can be considered as the first of a sequence of two hops. Since a non-returning second hop is an essential step for a large displacement of a particle, R_2 is closer to the structural relaxation rate and is a better characterization of the dynamics than R_1 as already demonstrated in Ref. [38]. Figure 13(b) plots the measured values together with R_1 from Fig. 6. It shows that both R_{ret} and R_2 admit surface enhancements. However, surface effects extend to the inner-surface layer only for R_2 but not noticeably for R_{ret} . This again illustrates the diverse penetration depths of surface effects on different dynam-

ical measurements and will be further discussed in the next section.

V. ORIGINS OF THE OUTER-, MID- AND INNER-SURFACE LAYERS

We have defined three sublayers of the surface mobile layer, which are color-shaded in plots of quantities against z in Figs. 1, 3(b), 6, 7, 12, 13(a)-(b) and 14 for easy comparison. The outer-surface layer defined in Sec. III is characterized by a reduced density ρ . We expect that the density reduction is simply due to the surface roughness and particle arrangements are already bulk-like right beneath the local position of the surface. This is supported by the good fit of ρ by Eq. (2) motivated by surfaces limited by surface tension [42]. A further support is from $g(r)$ in Fig. 2 in which the positions of the two subpeaks of the main peak coincide well with the energy minimized separations 0.96σ and 1.12σ of the bonded and non-bonded pair potentials. The subpeak positions remain unchanged even very close to the free surface. Structures are thus dominated by nearest neighboring interactions and are not significantly perturbed by missing further neighbors, as next nearest neighbor interactions are much weaker.

In Sec. IV, the mid-surface layer is characterized by a bulk-like ρ but an enhanced hopping rate R_1 . It can be understood qualitatively as follows. Particle motions at low temperature are dominated by micro-string hopping motions [57]. In each of these motions, l participating particles arranged linearly hop simultaneously to displace their adjacent neighbors within the micro-string. Generalizing for convenience to include the $l = 1$ case, all particle hops are considered as micro-string motions [53]. They constitute more general string-like motions [55] each of which in general comprises of multiple non-simultaneous micro-strings. Particle hopping motions in the form of micro-string motions have been considered as elementary motions in the structural relaxations of glassy systems [38, 53, 58], a view consistent with potential energy landscape (PEL) and activation energy barrier calculations [59]. Simultaneous hops of multiple particles in a micro-string can be favorable because the bonds between neighboring moving particles need not be broken.

We suggest that the enhancement of the hopping rate R_1 at the outer- and mid-surface layers is a simple consequence of surface effects on the PEL. A missing neighbor of a micro-string at the free surface in general alters the PEL and leads to a lower hopping energy barrier. Micro-string motions concerning at least one site at $z \gtrsim h_c - \sigma$ thus admit reduced barriers. Interpreting $h_c - \sigma - h_b = 3.25\sigma$ as the maximum lateral extent of micro-strings, only micro-strings located completely at $z \gtrsim h_b$ may be able to enjoy reduced barriers and thus an enhanced R_1 . The lengths of strings follow an exponential distribution with an average of about two particles long [60]. Micro-strings are their constituents and

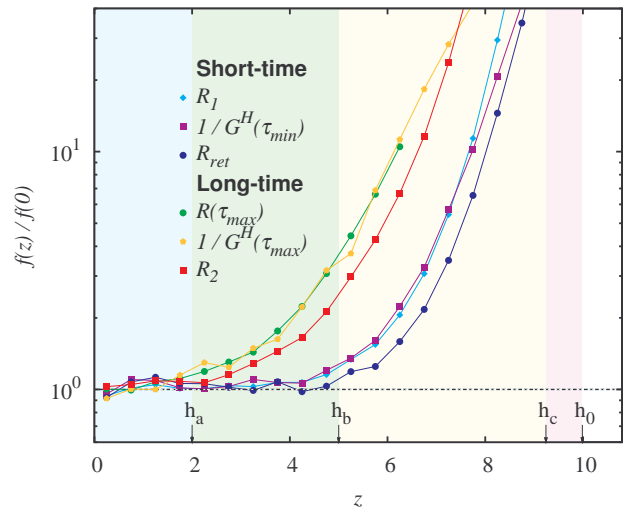


FIG. 14. Layer-resolved quantity $f(z)$ normalized with respect to bulk value $f(0)$ against coordinate z . Quantities shown include the net hopping rate $R(\tau)$ and the inverse correlation $1/G_H(\tau)$ at $\tau_{min} \equiv 20$ and $\tau_{max} \equiv 20480$, with $R_1 \equiv R(\tau_{min})$. Also shown are the rates R_{ret} and R_2 of particle returning and non-returning second hops.

are even shorter. A maximum lateral extent of 3.25σ assumed above should be reasonable.

From Fig. 7, the rather abrupt convergence of R_1 to its bulk value at $z \simeq h_b$ indicates that micro-string motions are very localized events depending only on the immediate neighborhood of the sites concerned. This implies that barriers based on, for instance, elastic models [61] with interactions typically decaying as power-laws may not be applicable. In contrast, the MSD at τ_{min} shows a much more gradual convergence to the bulk value. We suggest that this is because the MSD accounts for not only hopping but also elastic distortions. Specifically, when a particle hops, the structural perturbations can be represented by a force dipole which generates elastic distortions decaying with distance in a power-law [62]. This leads to creep motions (see Sec. IV A) of neighboring particles. Closer to the free surface, creep motions are more significant due to the much more numerous hops. This picture is supported by the observation from Fig. 4 that the displacement distribution $P(\Delta r)$ at the inner-surface layer differs from that in the bulk-like layer mainly by having more creep motions rather than hops as explained in Sec. IV A.

The inner-surface layer demonstrates that surface effects admit different penetration depths even for different dynamical measurements. The contrast in the penetration depths for R_1 and $R(\tau_{max})$ is already demonstrated in Fig. 7. As further examples of hopping related dynamics measurements, Fig. 14 replots R_1 and $R(\tau_{max})$ together with $1/G_H(\tau_{min})$, $1/G_H(\tau_{max})$, R_{ret} and R_2 after normalization by their bulk values. Note that R_{ret} and R_2 can be categorized respectively as short- and long-

time measurements based on the average waiting times of the corresponding processes. From Fig. 14, it is interesting to observe that the normalized quantities resemble each other in the respective groups of short- and long-time measurements. Moreover, one group differs from the other mainly by a shift along the z axis. Therefore, surface effects on all hopping related dynamical measurements studied in this work show distinct penetration depths in the short- and long-time regimes.

The normalized quantities in Fig. 7 are fitted to the empirical form

$$\frac{f(z)}{f(0)} = 1 + \exp\left(\frac{z - z_0}{\lambda_M}\right). \quad (17)$$

Here, λ_M is a characteristic width of the surface mobile layer as probed by the quantity $f(z)$ and z_0 is the position at which the surface effects become significant. The fits are good except for the MSD at τ_{min} as it only applies up to $f(z)/f(0) \lesssim 3$ compared to about 10 for the other cases. The different behavior of the MSD at τ_{min} is expected to be due to elastic distortions induced by hops at the surface as explained above. Focusing on the hopping statistics, we get $\lambda_M = 0.67\sigma$ and $z_0 = 6.4\sigma$ for $f(z) = R_1$, while $\lambda_M = 0.95\sigma$ and $z_0 = 4.2\sigma$ for $f(z) = R(\tau_{max})$. The difference between the two values of z_0 hence provide a more accurate estimate of 2.2σ for the thickness of the inner-surface layer, which is consistent with the thickness 2.0σ adopted above. Other quantities shown in Fig. 14 can also be well fitted to Eq. (17). Equation (17) can be rewritten as $f(z) = f(0) + f(0)\exp((z - z_0)/\lambda_M)$. The two terms physically account for events intrinsic to the bulk and induced by the free surface respectively. The exponential decay may be a consequence of the exponential distribution of the lengths of the strings [60].

The exponential form followed by $R(\tau_{max})$ in Eq. (17) defines a mobility profile for long-time motions. It is expected to be the cause of a related exponential profile followed by the layer-resolved flow velocity under steady-state driven conditions reported in Ref. [30]. The characteristic decay width $\lambda_M = 0.95\sigma$ obtained above for $R(\tau_{max})$ indeed agrees very well with the corresponding width of $\lambda_M = 0.94\sigma$ for the flow velocity profile from Ref. [30].

In the inner-surface layer, we thus observe the co-existence of a bulk-like R_1 with enhanced mobility. This seemingly contradictory phenomena can be better understood based on the probabilities P_{ret} and P_2 of returning and non-return second hops. From Fig. 13(a), a high value of P_{ret} is observed in the bulk-like layer, implying a significant slowdown due to strong anti-correlations in the hopping motions. At the inner-surface layer, P_{ret} is comparatively lower indicating reduced anti-correlations in particle hops and thus enhanced mobility. This reduction of anti-correlations is also reflected quantitatively in g^H and G^H as well as visually in the dynamic heterogeneity. The enhanced mobility in the inner-surface layer hence results from diminished hopping anti-correlations

rather than more frequent hops.

VI. FACILITATION VIA DIMINISHING HOPPING ANTI-CORRELATIONS

Widely studied theories of glass include the Adam-Gibbs theory [63], mode-coupling theory [64], dynamic facilitation theory [65–70], random first order transition theory [71], elastic models [61] and so on. We have shown above that anti-correlations in hopping events are important in understanding surface enhanced mobility. Theories emphasizing the importance of correlations in elementary motions such as the facilitation picture [65–70] are most promising in describing our findings.

Dynamic facilitation often describes the phenomenon that motions in a local region can initiate other subsequent motions in a neighboring local region [3]. As is visually evident from Fig. 8, the abundant motions close to the free surface facilitate motions deeper in the film. For the inner-surface layer where the hopping rate is already bulk-like, enhanced motions result from facilitation by the extra motions in the mid-surface layer. However, the facilitation does not increase the rate of hopping motions in the inner-surface layer, which is essentially fixed by the bulk-like PEL. Instead, it acts by suppressing the anti-correlations between hopping events. Therefore, according to our results, dynamic facilitation is in fact the phenomenon that motions in a local region reduce the anti-correlations between motions in a neighboring local region and thus enhance structural relaxations.

Motivated by these findings, we have recently identified a micro-string interaction process as the dynamic facilitation mechanism consistent with the above requirements [38]. An analytical study leads to a local random configuration tree theory of glass [70] which is illustrated by explicit calculations applied to a distinguishable particle lattice model (DPLM) [69]. In this picture, micro-string motions are initiated by quasi-voids, each of which consists of neighboring free volumes transported in whole by a micro-string motion [38]. At low temperature, such voids are predominately trapped by the PEL to within finite regions in the configuration space and this induces the strong anti-correlations of the particle hopping motions. A micro-string motion initiated by a void perturbs the PEL experienced by other voids, which are then momentarily untrapped or, more precisely, trapped differently. This thus breaks the hopping anti-correlations without generating additional micro-string motions as is required by observations in this work. At the outer- and mid-surface layers, voids are more mobile due to surface effects on the PEL. This provides the voids in the inner-surface layer with a relatively free boundary condition at the interface to the mid-surface layer. Additional void untrapping events and enhanced dynamics thus result.

VII. DISCUSSIONS

In summary, polymer films with free surfaces are simulated and analyzed in detail. We have studied structural properties including density and particle pair distribution function, as well as dynamical properties including mean square displacement, displacement distribution, particle hopping rate, long-time net hopping rate, hopping event pair distribution function, and particle returning and non-returning hopping probabilities and rates. Surface effects on particle hopping rate are qualitatively different from those on mean square displacement and terminate abruptly when going into the film. Based on the penetration depths of surface effects on respectively the film density, hopping rate, and long-time net hopping rate, we define the outer-, mid- and inner-sublayers of the surface mobile layer. The inner-surface layer shows a bulk-like particle hopping rate but an enhanced mobility. The enhanced mobility results from reduced temporal anti-correlations of particle hops associated with a reduced dynamic heterogeneity. The observation suggests that dynamic facilitation acts by diminishing the anti-correlations rather than enhancing the rate of elementary motions.

We have reported results at $T = 0.36$, which is the lowest temperature accessible for equilibrium simulations. Smaller scale simulations at higher T and non-equilibrium simulations at lower T indicate that as T decreases, the net hopping rate $R(\tau)$ at the surface drops more mildly than in the bulk. Surface enhancement of the mobility thus increases. The exponential decay in Eq. (17) however admits a slightly reduced characteristic width λ_M . Overall, results are qualitatively similar to those reported above and there is only a weak T dependence of the mobile layer thickness. In this work, we have studied short-chain polymer melts in this work. However, we expect that the diverse penetration depths of surface effects and the peculiar properties of the inner-surface layer may also be qualitatively applicable to other glassy systems with dynamics dominated by particle hops. Further studies on these systems will be of great interest.

Appendix A: Layer resolution schemes

When performing layer-resolved dynamical measurements concerning the displacement $\mathbf{r}_i(t_0 + \tau) - \mathbf{r}_i(t_0)$ in Eqs. (6) and (11), we assume that particle i is in layer Ω_z solely based on its initial position $\mathbf{r}_i(t_0)$ at the beginning of the duration τ . This provides good statistics, consistency with bulk values, and convenience in possible analytical calculations in the future. Since the final position $\mathbf{r}_i(t_0 + \tau)$ may be at a neighboring layer, this scheme in principle may provide only limited sharpness in the layer-resolution. However, we have checked that adopting two other more stringent layer-resolution criteria does not alter our results qualitatively. A main reason is that we focus mainly on hopping statistics and onset

of surface perturbations concerning in most cases rather small displacements.

Specifically, we have also considered i in Ω_z only if both the initial and the final positions $\mathbf{r}_i(t_0)$ and $\mathbf{r}_i(t_0 + \tau)$ are in Ω_z . The resulting layer-resolved MSD is similar to that in Fig. 3(a). Alternatively, we consider i in Ω_z only if $\mathbf{r}_i(t)$ during the whole period (i.e. $t_0 \leq t < t_0 + \tau$) is in Ω_z , up to a time resolution limited by our recorded trajectories. This is very similar to the approach used in Ref. [12]. The MSD hence obtained is shown in Fig. 15. The statistics nevertheless deteriorate since the sample sizes are much reduced. Yet, compared with that in Fig. 3, values are similar when the MSD is small. More importantly, the penetration depths of the surface effects are similar.

Adopting again the condition that both the initial and the final positions must be in Ω_z , we have also calculated the net particle hopping rate $R(\tau)$ and the hopping event correlation $G^H(\tau)$. Both sets of results are qualitatively similar to those in Figs. 6 and 12 respectively and the validity of the simple layer-resolving algorithm adopted in the main text is readily verified.

Acknowledgments

We thank Ophelia Tsui, Fathollah Varnik, Jörg baschnagel, Simone Napolitano and Patrick Charbonneau for helpful discussions. We are grateful to the support of Hong Kong GRF (Grant 15330516).

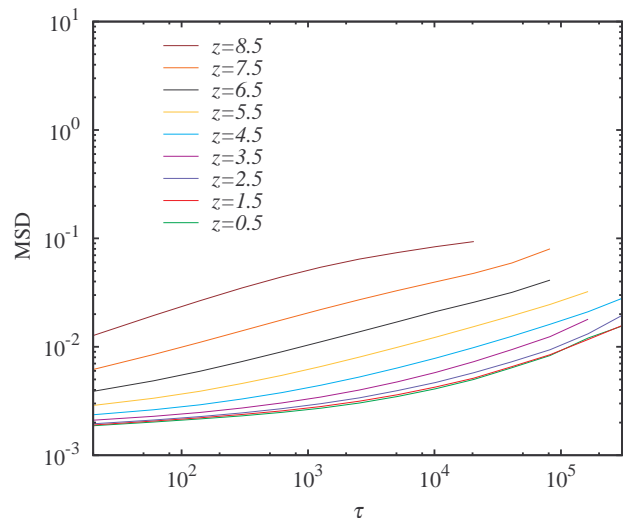


FIG. 15. Mean square displacement (MSD) similar to that shown in Fig. 3(a) except for different layer-resolution criteria. Particles considered must be inside layer Ω_z at all time during the period τ .

-
- [1] E. Donth, *The glass transition: relaxation dynamics in liquids and disordered materials*, Vol. 48 (Springer, 2001)
- [2] K. Binder and W. Kob, *Glassy materials and disordered solids: An introduction to their statistical mechanics* (World Scientific, 2011)
- [3] G. Biroli and J. P. Garrahan, “Perspective: The glass transition,” *J. Chem. Phys.* **138**, 12A301 (2013)
- [4] F. H. Stillinger and P. G. Debenedetti, “Glass transition thermodynamics and kinetics,” *Annu. Rev. Condens. Matter Phys.* **4**, 263 (2013)
- [5] M. D. Ediger and P. Harrowell, “Perspective: Supercooled liquids and glasses,” *J. Chem. Phys.* **137**, 080901 (2012)
- [6] M. D. Ediger and J. A. Forrest, “Dynamics near free surfaces and the glass transition in thin polymer films: a view to the future,” *Macromolecules* **47**, 471 (2013)
- [7] F. Chen, C.-H. Lam, and O. K. C. Tsui, “The surface mobility of glasses,” *Science* **343**, 975 (2014)
- [8] S. Napolitano, E. Glynos, and N. B. Tito, “Glass transition of polymers in bulk, confined geometries, and near interfaces,” *Rep. Prog. Phys.* **80**, 036602 (2017)
- [9] J. L. Keddie, R. A. L. Jones, and R. A. Cory, “Size-dependent depression of the glass transition temperature in polymer films,” *Europhys. Lett.* **27**, 59 (1994)
- [10] S. Kawana and R. A. L. Jones, “Character of the glass transition in thin supported polymer films,” *Phys. Rev. E* **63**, 021501 (2001)
- [11] S. Peter, H. Meyer, and J. Baschnagel, “Thickness-dependent reduction of the glass-transition temperature in thin polymer films with a free surface,” *J. Polym. Phys. B* **44**, 2951 (2006)
- [12] S. Peter, H. Meyer, J. Baschnagel, and R. Seemann, “Slow dynamics and glass transition in simulated free-standing polymer films: a possible relation between global and local glass transition temperatures,” *J. Phys. Condens. Matter* **19**, 205119 (2007)
- [13] Z. Yang, Y. Fujii, F. K. Lee, C. H. Lam, and O. K. C. Tsui, “Glass transition dynamics and surface layer mobility in unentangled polystyrene films,” *Science* **328**, 1676 (2010)
- [14] L. Zhu, C. W. Brian, S. F. Swallen, P. T. Straus, M. D. Ediger, and L. Yu, “Surface self-diffusion of an organic glass,” *Phys. Rev. Lett.* **106**, 256103 (2011)
- [15] Y. Chai, T. Salez, J. D. McGraw, M. Benzaquen, K. Dalnoki-Veress, E. Raphaël, and J. A. Forrest, “A direct quantitative measure of surface mobility in a glassy polymer,” *Science* **343**, 994 (2014)
- [16] T. Kajiyama, K. Tanaka, N. Satomi, and A. Takahara, “Surface relaxation process of monodisperse polystyrene film based on lateral force microscopic measurements,” *Macromolecules* **31**, 5150 (1998)
- [17] Z. Fakhraai and J. A. Forrest, “Measuring the surface dynamics of glassy polymers,” *Science* **319**, 600 (2008)
- [18] S. Herminghaus, “Polymer thin films and surfaces: Possible effects of capillary waves,” *Eur. Phys. J. E* **8**, 237 (2002)
- [19] D. Long and F. Lequeux, “Heterogeneous dynamics at the glass transition in van der Waals liquids, in the bulk and in thin films,” *Eur. Phys. J. E* **4**, 371 (2001)
- [20] S. T. Milner and J. E. G. Lipson, “Delayed glassification model for free-surface suppression of t_g in polymer glasses,” *Macromolecules* **43**, 9865 (2010)
- [21] P. Z. Hanakata, J. F. Douglas, and F. W. Starr, “Interfacial mobility scale determines the scale of collective motion and relaxation rate in polymer films,” *Nat. Comm.* **5**, 4163 (2014)
- [22] T. Salez, J. Salez, K. Dalnoki-Veress, E. Raphaël, and J. A. Forrest, “Cooperative strings and glassy interfaces,” *Proc. Natl. Acad. Sci.* **112**, 8227 (2015)
- [23] K. Paeng, S. F. Swallen, and M. D. Ediger, “Direct measurement of molecular motion in freestanding polystyrene thin films,” *J. Am. Chem. Soc.* **133**, 8444 (2011)
- [24] R. N. Li, F. Chen, C.-H. Lam, and O. K. C. Tsui, “Viscosity of pmma on silica: Epitome of systems with strong polymer–substrate interactions,” *Macromolecules* **46**, 7889 (2013)
- [25] J. E. Pye, K. A. Rohald, E. A. Baker, and C. B. Roth, “Physical aging in ultrathin polystyrene films: Evidence of a gradient in dynamics at the free surface and its connection to the glass transition temperature reductions,” *Macromolecules* **43**, 8296 (2010)
- [26] W. Ogieglo, K. Tempelman, S. Napolitano, and N. E. Benes, “Evidence of a transition layer between the free surface and the bulk,” *J. Phys. Chem. Letters* **9**, 1195 (2018)
- [27] I. McKenzie, Y. Chai, D. L. Cortie, J. A. Forrest, D. Fujimoto, V. L. Karner, R. F. Kiefl, *et al.*, “Direct measurements of the temperature, depth and processing dependence of phenyl ring dynamics in polystyrene thin films by β -detected NMR,” *Soft Matter* (2018)
- [28] T. S. Jain and J. J. de Pablo, “Investigation of transition states in bulk and freestanding film polymer glasses,” *Phys. Rev. Lett.* **92**, 155505 (2004)
- [29] P. Z. Hanakata, J. F. Douglas, and F. W. Starr, “Local variation of fragility and glass transition temperature of ultra-thin supported polymer films,” *J. Chem. Phys.* **137**, 244901 (2012)
- [30] C.-H. Lam and O. K. C. Tsui, “Crossover to surface flow in supercooled unentangled polymer films,” *Phys. Rev. E* **88**, 042604 (2013)
- [31] K. Kremer and G. S. Grest, “Dynamics of entangled linear polymer melts: A molecular-dynamics simulation,” *J. Chem. Phys.* **92**, 5057 (1990)
- [32] F. Varnik, J. Baschnagel, and K. Binder, “Reduction of the glass transition temperature in polymer films: A molecular-dynamics study,” *Phys. Rev. E* **65**, 021507 (2002)
- [33] F. Varnik and K. Binder, “Shear viscosity of a supercooled polymer melt via nonequilibrium molecular dynamics simulations,” *J. Chem. Phys.* **117**, 6336 (2002)
- [34] R. Auhl, R. Everaers, G. S. Grest, K. Kremer, and S. J. Plimpton, “Equilibration of long chain polymer melts in computer simulations,” *J. Chem. Phys.* **119**, 12718 (2003)
- [35] P. Scheidler, W. Kob, and K. Binder, “The relaxation dynamics of a supercooled liquid confined by rough walls,” *J. Phys. Chem. B* **108**, 6673 (2004)
- [36] A. R. C. Baljon, M. H. M. Weert Van, R. B. DeGraaff, and R. Khare, “Glass transition behavior of polymer films of nanoscopic dimensions,” *Macromolecules* **38**, 2391 (2005)
- [37] H. Morita, K. Tanaka, T. Kajiyama, T. Nishi, and

- M. Doi, "Study of the glass transition temperature of polymer surface by coarse-grained molecular dynamics simulation," *Macromolecules* **39**, 6233 (2006)
- [38] C.-H. Lam, "Repetition and pair-interaction of string-like hopping motions in glassy polymers," *J. Chem. Phys.* **146**, 244906 (2017)
- [39] J.-X. Hou, C. Svaneborg, R. Everaers, and G. S. Grest, "Stress relaxation in entangled polymer melts," *Phys. Rev. Lett.* **105**, 068301 (2010)
- [40] M. Doi and S. F. Edwards, *The theory of polymer dynamics* (Oxford University Press, 1986)
- [41] J. A. Anderson, C. D. Lorenz, and A. Travesset, "General purpose molecular dynamics simulations fully implemented on graphics processing units," *J. Comp. Phys.* **227**, 5342 (2008)
- [42] D. Nelson, T. Piran, and S. Weinberg, *Statistical mechanics of membranes and surfaces* (World Scientific, 2004)
- [43] J.-P. Hansen and I. R. McDonald, *Theory of simple liquids* (Elsevier, 1990)
- [44] Göran Wahnström, "Molecular-dynamics study of a supercooled two-component lennard-jones system," *Phys. Rev. A* **44**, 3752 (1991)
- [45] H. Miyagawa, Y. Hiwatari, B. Bernu, and J. P. Hansen, "Molecular dynamics study of binary soft-sphere mixtures: Jump motions of atoms in the glassy state," *J. Chem. Phys.* **88**, 3879 (1988)
- [46] K. Vollmayr-Lee, "Single particle jumps in a binary lennard-jones system below the glass transition," *J. Chem. Phys.* **121**, 4781 (2004)
- [47] M. Vogel, "Conformational and structural relaxations of poly (ethylene oxide) and poly (propylene oxide) melts: Molecular dynamics study of spatial heterogeneity, cooperativity, and correlated forward-backward motion," *Macromolecules* **41**, 2949 (2008)
- [48] T. Kawasaki and A. Onuki, "Slow relaxations and string-like jump motions in fragile glass-forming liquids: Breakdown of the stokes-einstein relation," *Phys. Rev. E* **87**, 012312 (2013)
- [49] J. W. Ahn, B. Falahee, C. D. Piccolo, M. Vogel, and D. Bingemann, "Are rare, long waiting times between rearrangement events responsible for the slowdown of the dynamics at the glass transition?," *J. Chem. Phys.* **138**, 12A527 (2013)
- [50] J. Helfferich, F. Ziebert, S. Frey, H. Meyer, J. Farago, A. Blumen, and J. Baschnagel, "Continuous-time random-walk approach to supercooled liquids. i. different definitions of particle jumps and their consequences," *Phys. Rev. E* **89**, 042603 (2014)
- [51] H.-B. Yu, R. Richert, and K. Samwer, "Structural rearrangements governing johari-goldstein relaxations in metallic glasses," *Sci. Adv.* **3**, e1701577 (2017)
- [52] Y. J. Lü and W. H. Wang, "Single-particle dynamics near the glass transition of a metallic glass," *Phys. Rev. E* **94**, 062611 (2016)
- [53] A. S. Keys, L. O. Hedges, J. P. Garrahan, S. C. Glotzer, and D. Chandler, "Excitations are localized and relaxation is hierarchical in glass-forming liquids," *Phys. Rev. X* **1**, 021013 (2011)
- [54] L. Berthier, G. Biroli, J.-P. Bouchaud, L. Cipelletti, and W. van Saarloos, *Dynamical heterogeneities in glasses, colloids, and granular media*, Vol. 150 (Oxford University Press, 2011)
- [55] C. Donati, J. F. Douglas, W. Kob, S. J. Plimpton, P. H. Poole, and S. C. Glotzer, "Stringlike cooperative motion in a supercooled liquid," *Phys. Rev. Lett.* **80**, 2338 (1998)
- [56] C. Donati, S. C. Glotzer, P. H. Poole, W. Kob, and S. J. Plimpton, "Spatial correlations of mobility and immobility in a glass-forming lennard-jones liquid," *Phys. Rev. E* **60**, 3107 (1999)
- [57] Y. Gebremichael, M. Vogel, and S. C. Glotzer, "Particle dynamics and the development of string-like motion in a simulated monoatomic supercooled liquid," *J. Chem. Phys.* **120**, 4415 (2004)
- [58] M. P. Ciamarra, R. Pastore, and A. Coniglio, "Particle jumps in structural glasses," *Soft matter* **12**, 358 (2016)
- [59] S. Swayamjyoti, J. F. Löffler, and P. M. Derlet, "Local structural excitations in model glasses," *Phys. Rev. B* **89**, 224201 (2014)
- [60] M. Aichele, Y. Gebremichael, F. W. Starr, J. Baschnagel, and S. C. Glotzer, "Polymer-specific effects of bulk relaxation and stringlike correlated motion in the dynamics of a supercooled polymer melt," *J. Chem Phys.* **119**, 5290 (2003)
- [61] J. C. Dyre, "Colloquium: The glass transition and elastic models of glass-forming liquids," *Rev. Mod. Phys.* **78**, 953 (2006)
- [62] A. Pimpinelli and J. Villain, *Physics of crystal growth*, Vol. 19 (Cambridge university press Cambridge, 1998)
- [63] G. Adam and J. H. Gibbs, "On the temperature dependence of cooperative relaxation properties in glass-forming liquids," *J. Chem Phys.* **43**, 139 (1965)
- [64] W. Götze, *Complex dynamics of glass-forming liquids: a mode-coupling theory* (Oxford University Press, 2008)
- [65] G. H. Fredrickson and H. C. Andersen, "Kinetic ising model of the glass transition," *Phys. Rev. Lett.* **53**, 1244 (1984)
- [66] R. G. Palmer, D. L. Stein, E. Abrahams, and P. W. Anderson, "Models of hierarchically constrained dynamics for glassy relaxation," *Phys. Rev. Lett.* **53**, 958 (1984)
- [67] F. Ritort and P. Sollich, "Glassy dynamics of kinetically constrained models," *Adv. Phys.* **52**, 219 (2003)
- [68] J. P. Garrahan, P. Sollich, and C. Toninelli, "Kinetically constrained models," in *Dynamical Heterogeneities in Glasses, Colloids and Granular Media*, edited by L. Berthier, G. Biroli, J.-P. Bouchaud, L. Cipelletti, and W. van Saarloos (Oxford University Press, 2011)
- [69] L.-H. Zhang and C.-H. Lam, "Emergent facilitation behavior in a distinguishable-particle lattice model of glass," *Phys. Rev. B* **95**, 184202 (2017)
- [70] C.-H. Lam, "Local random configuration-tree theory for string repetition and facilitated dynamics of glass," *J. Stat. Mech.* **2018**, 023301 (2018)
- [71] T. R. Kirkpatrick, D. Thirumalai, and P. G. Wolynes, "Scaling concepts for the dynamics of viscous liquids near an ideal glassy state," *Phys. Rev. A* **40**, 1045 (1989)